Strong gradient of benthic biogeochemical processes along a macrotidal temperate estuary: focus on P and Si cycles

Mélanie Raimonet, Françoise Andrieux-Loyer, Olivier Ragueneau, Emma Michaud, Roger Kérouel, Xavier Philippon, Michel Nonent, Laurent Mémery

Strong gradient of benthic biogeochemical processes along a macrotidal temperate estuary: focus on P and Si cycles

Mélanie Raimonet[a]*, Françoise Andrieux-Loyer[b], Olivier Ragueneau[a], Emma Michaud[a], Roger Kerouel[b], Xavier Philippon[b], Michel Nonent[c], Laurent Mémery[a]

[a] *Laboratoire des Sciences de l'Environnement Marin, UMR 6539, Institut Universitaire Européen de la Mer, Plouzané, France*

[b] *DYNECO Pelagos, IFREMER, Plouzané, France*

[c] *Service de Radiologie et Imagerie Médicale, CHU Brest et GETBO, Faculté de Médecine et des Sciences de la Santé, UBO, Brest, France*

* Corresponding author: melanie.raimonet@gmail.com

Current address: UMR 7619 Sisyphe, Université Pierre et Marie Curie Paris VI, Paris, France

Abstract

This study aims to investigate the role of spatial and temporal physical, biological and biogeochemical gradients on sediment biogeochemistry along a macrotidal and Si-rich estuary. Scanning and biogeochemical analyses were performed in the inner, mid and outer Aulne Estuary (France) at four seasons. The inner estuary shows high diagenetic activity linked to fluid mud dynamics and river loads. The highest authigenic phosphorus (Aut-P) concentrations ever found in the literature are observed in the inner estuary (18 µmol g^{-1} PS sediment). This is explained by a combination of favorable factors, i.e. the high organic matter and nutrient loads, the reductive conditions, the freshwater properties (low pH, OH^-, sulfate and Mg^{2+} concentrations), the increase of particle residence time by the upward convergence of particles due to residual currents, and allochthonous riverine Aut-P. We suggest that the high $Si(OH)_4$ concentrations (> 400 µM) may even increase Aut-P precipitation through the increase of Fe-P formation in these low salinity conditions. In the mid estuary, erosion-deposition dynamics dominate in point bars and lead to the succession of poor and rich organic and authigenic phosphorus layers, recording thus the seasonality of matter loads and its seasonal translocation from the inner estuary. In the outer estuary, deposition rates are high and constant and biogeochemical properties are characteristic of marine environments. The precipitation of Aut-P from free phosphate (PO_4^{3-}) is lower than in the inner estuary and might be limited by higher Mg^{2+} concentrations in saline waters. This study highlights that small macrotidal estuaries, and especially their freshwater sediments, may constitute an important phosphorus sink through the precipitation of Aut-P. This precipitation could even be enhanced in fresh or brackish environments, thus increasing long

term phosphorus storage and altering benthic fluxes of PO_4^{3-} to the pelagic ecosystem.

Keywords: early diagenesis, silicate, phosphate, authigenic phosphorus, macrotidal, estuary

1. Introduction

Over the past century, estuarine and coastal ecosystems have suffered eutrophication in response to increased anthropogenic loads of nitrogen (N) and phosphorus (P) (Nixon 1995; Seitzinger et al. 2005). Eutrophication has led to drastic changes in N:P:Si ratios and ecosystem functioning (Cloern 2001; Ragueneau et al. 2002), resulting in seasonal limitations of phytoplankton growth by N, P and/or silicon (Si) (Conley 2000; Beucher et al. 2004). During the last decades, P and N have been identified to limit phytoplankton growth in fresh and marine waters, respectively (Smith 1984; Howarth and Marino 2006). Si and P limitations are now implicated in estuarine and coastal waters (Howarth et al. 2011) in response to Si retention - due to river damming (Conley et al. 1993) - and P removal - associated to the improvement in sewage treatment plants (Némery and Garnier 2006).

Nutrient loads and limitations not only depend on riverine fluxes, but also on benthic-pelagic coupling. In shallow ecosystems such as estuaries, benthic sediments constitute either 1) a nutrient source through the mineralization of deposited biogenic matter and diffusion processes generating benthic fluxes, and/or 2) a sink of deposited - allochthonous and/or autochthonous - biogenic matter (Prastka et al. 1998; Soetaert et al. 2000; Laruelle 2009). It is therefore very important to study the relative fate of N, P and Si upon the deposition of organic matter at the sediment-water interface, in particular in shallow ecosystems e.g. estuaries.

Along the land-sea continuum, estuaries are among the most productive ecosystems, but also the most hydrologically variable ones, due to river discharge, tides and winds (Day et al. 1989; Cloern 2001; Aller 2004). As tides can lead to a succession of different sedimentary facies

in estuaries (Aller 1994), it is essential to determine the sedimentary properties that exert a profound influence on vertical distributions of chemical species. Estuaries are also characterized by sharp gradients of environmental conditions - pH, salinity, temperature, nutrient concentrations - which can lead to strong gradients of biogeochemical processes (Yamada and D'Elia 1980; Sharp et al. 1984), but also to interactions between biogeochemical cycles, e.g. between P and Si cycles (Tallberg et al. 2008).

Estuaries play a major role in the transport and transformation of key elements (e.g. P and Si) and their bioavailability in the coastal zone. Estuaries are characterized by high buffering capacity due to the quick adsorption and desorption of dissolved inorganic P (phosphate, PO_4^{3-}) onto and from particles (Froelich 1988; Sundby et al. 1992), which permit the transport of adsorbed PO_4^{3-} along the land-sea continuum and its progressive release in brackish and marine waters. The deposition and mineralization of organic P (Orga-P) also generates PO_4^{3-} in sediment pore waters. In oxic sediment, PO_4^{3-} quickly adsorbs onto mineral particles, and reacts with iron oxides to form iron-bound phosphorus (Fe-P), thus buffering benthic PO_4^{3-} fluxes to the water column (Sundby et al. 1992; Anschutz et al. 1998). In deep and anoxic sediments, Orga-P mineralization and Fe-P dissolution generate PO_4^{3-} which can precipitate - e.g., with Ca^{2+} - to form a less reactive authigenic phase (Aut-P) favoring P storage (Ruttenberg and Berner 1993; Slomp et al. 1996). However, Aut-P is not often measured and accounts for a small fraction of P in existing estuarine studies.

The Si cycle is generally less studied than N or P cycles in estuaries. The availability in dissolved Si (silicic acid, $Si(OH)_4$) is however essential for the growth of diatoms, which constitute 50-75 % of coastal phytoplankton production (Nelson et al. 1995). The incorporation

of Si by living organisms also participates in increasing the deposition rate of organic matter through the ballast effect of amorphous biogenic silica (Smetacek 1985). The amorphous silica - e.g., diatom skeleton, sponges, plants - settles at the sediment-water interface and dissolves into $Si(OH)_4$ that diffuses back to pelagic waters. As with PO_4^{3-}, $Si(OH)_4$ also undergoes sorption processes onto particles, in particular in resuspended sediments (Gehlen and Van Raaphorst 2002).

Estuaries have however been given low attention with respect to Si-P interactions. Competition between Si and P cycles - i.e., between $Si(OH)_4$ and PO_4^{3-} for sorption sites - were suggested in lakes, rivers and/or laboratory conditions (Hartikainen et al. 1996; Tuominen et al. 1997; Mayer and Jarrell 2000; Koski-Vähälä et al. 2001). $Si(OH)_4$ was shown to enhance PO_4^{3-} desorption and benthic fluxes (Mayer and Jarrell 2000; Koski-Vähälä et al. 2001), prevent PO_4^{3-} adsorption, but also increase iron-bound P (Fe-P) formation (Mayer and Jarrell 2000; Koski-Vähälä et al. 2001; Loucaides et al. 2010). Because high concentrations of $Si(OH)_4$ could alter the P cycle, it is essential to investigate simultaneously benthic chemical species of Si and P cycles, and to consider and discuss the impact of Si-P interactions on the biogeochemistry of Si-enriched benthic sediments. Importantly, the role of $Si(OH)_4$ has never been related to authigenic P (Aut-P) formation.

The Aulne Estuary - the main tributary flowing into the Bay of Brest (Fig. 1) - is a shallow macrotidal ecosystem characterized by high anthropogenic nutrient inputs (due to intense agricultural activities, fisheries and urbanization), Si inputs resulting from weathering of Si-enriched soils and terrestrial phytoliths, and intense hydrodynamic regime (e.g. high tidal range and currents). These properties of the Aulne Estuary may be favorable for Si-P interactions, as

recently suggested by the increased PO_4^{3-} benthic fluxes linked to high $Si(OH)_4$ concentrations of the Bay of Brest (Tallberg et al. 2008).

The aim of this study was to investigate the role of environmental factors on the benthic biogeochemical processes and the distribution of P and Si forms along an estuarine gradient. This study was undertaken in benthic sediments of the Aulne Estuary, as a model of $Si(OH)_4$ enriched sediments in a small macrotidal estuary.

2. Methods

2.1. Study site

Located in Northwestern France, the macrotidal Aulne Estuary (averaged tidal amplitude of 4 m, 35 km long; Fig. 1) receives N and Si enriched waters from the Aulne River that drains an area of about 1800 km² and brings annually 60 % of fresh water to the Bay of Brest. Nitrate (NO_3^-) concentrations at the Aulne River outfall were maximal in winter (~ 500 µmol L^{-1}) and minimal in summer (~ 100 µM; Réseau ECOFLUX, http://www-iuem.univ-brest.fr/ecoflux; Table 1). Free PO_4^{3-} concentrations through the year were consistently low (~ 1 µM; Réseau ECOFLUX; Table 1) due to PO_4^{3-} adsorption onto particles (Mayer and Gloss 1980). Mean $Si(OH)_4$ concentrations were close to 130 µM with sporadic variations between 50 and 200 µM (Réseau ECOFLUX; Table 1). The oceanic climate of the region leads to higher precipitations - associated to frequent storms - in winter than in summer, thus modifying river discharge. In 2009, river flow ranged from 1.7 to 189 $m^3 s^{-1}$ (mean = 24.4 $m^3 s^{-1}$; Fig. 2). The spatial distribution of

125 salinity ranging from 0 to 35 throughout the Aulne Estuary depends on season, river discharge
126 and tide. The concentrations of NO_3^-, PO_4^{3-} and $Si(OH)_4$ decreased with salinity (Table 1) to 0-
127 35, 0-0.5, and 0-10 µM, respectively, in the Bay of Brest (Service d'Observation en Milieu
128 Littoral SOMLIT, somlit.epoc.u-bordeaux1.fr).

129

130 2.2. Sampling design

131

132 Cruises were performed in February, May, July and October 2009. Three stations were
133 located from upstream to downstream of the Aulne Estuary (A1, A2, A3; Fig. 1) at salinity of ~
134 0, ~ 20 and ~ 30. Sampling was always performed at mid-tide (+/- 1.5 h) in subtidal shores. Note
135 that the presence of highly consolidated and unpenetrable sediment at station A2 previously
136 sampled in February and May prevented core sampling at the exactly same site in July and
137 October. Core sampling was consequently performed 200 m downward the site previously
138 sampled in February and May.

139 Gravity corer (UWITEC®) was used to sample plexiglass cores (9.5 cm diameter x 60 cm
140 long). Corer weight was adjusted to allow 30 cm penetration into the sediment without disturbing
141 the sediment-water interface.

142 Two sediment cores were sampled at each station in February, July and October - but not
143 in May - to characterize the sedimentary structure by using Computer axial tomography (CAT
144 scan). These cores were exposed to aerated waters in laboratory prior to their analysis. Three
145 other cores were sampled at each station in February, May, July and October for assessment of

benthic biogeochemistry. These sediment cores were immediately sliced at a resolution of 0.5 cm (0-2 cm depth), 1 cm (2-4 cm depth), 2 cm (4-12 cm depth), and 4 cm (12-20 cm depth). Sediment sections were placed in sealed 50-ml centrifuge tubes containing Vectaspin 20 filters (0.45 µm pore size, Whatman®) according to Andrieux-Loyer et al. (2008).

Interstitial waters were extracted by centrifuging the sub-sampled sediments at 3500 rpm for 10 min (2 times) at cooled temperature and later acidified to pH = 2. One aliquot of the extracted pore water was preserved at 4 °C for analyses of $Si(OH)_4$*, Fe^{2+} and Mn^{2+} concentrations and the other aliquot was frozen for PO_4^{3-}†, NH_4^+ and (NO_3^- + NO_2^-) analyses (Andrieux-Loyer et al. 2008).

Comparisons were performed between our technique (pore waters extracted from sediments, centrifuged in a Vectaspin tube, and acidified) and Rhizons® (without any contact with air). The two extraction techniques showed similar results in Fe^{2+} concentrations, confirming that quick core slicing, centrifuging, acidification, and storage gave confident concentrations of dissolved species, and thus in particulate P forms.

The bulk sediment samples that were not centrifuged were stored at 4 °C for less than 15 days to determine granulometry. Centrifuged sediments were freeze-dried during 48 h, put at 60 °C to ensure the complete sediment dryness, and ground for further analyses of P forms in the solid fraction.

2.3. Laboratory analyses

* Silicate (or orthosilicic acid) is noted $Si(OH)_4$ for simplification and is mainly present as H_4SiO_4.

† Inorganic phosphate (or orthophosphate) is noted PO_4^{3-} for simplification. The predominant forms are HPO_4^{2-} and $H_2PO_4^-$ in fresh and marine waters.

166

167 The cores were analyzed with a Philips scanner (MX 8000 IDT 16) between 3 and 6 days
168 after their sampling. Core tops were sealed with paraffin for stabilizing sediment according to
169 Michaud et al. (2003) in the morning before the analysis. During the analysis, cores were
170 horizontally placed on a table sliding through a crown consisting of a rotating X-ray source with
171 x vertical receptors. The principle of this technique has been widely described in the literature
172 (e.g., De Montety et al. 2003; Michaud et al. 2003). Core slices of 1 mm overlapping every 0.5
173 mm were scanned with the power settings of 120 Kv, 45 mA and a pitch of 1. We used a matrix
174 of 512 × 512 and the field of view was 115, which gave a pixel resolution on each transverse
175 section of 0.22 mm. The 2D longitudinal sections, which were perpendicularly reconstructed
176 from the transverse sections, had a pixel resolution of 1 mm.

177 Sediment grain size analyses were performed using LS 200 Beckman Coulter laser
178 granulometry. The fraction of fine particles - silt and clay (< 63 µm) - was chosen to characterize
179 sediment granulometry (Lesourd et al. 2003). Porosity was obtained after drying wet sediment of
180 precise volume for 5 days, when the loss of weight was determined (Berner 1980).

181 P forms expressed in µmol g^{-1} were determined using the sequential analytical procedure
182 detailed in Andrieux-Loyer et al. (2008) and adapted from widespread extraction methods
183 (Psenner et al. 1988; Ruttenberg 1992; Aspila 1976). Adsorbed and iron-oxide bound P (Fe-P)
184 was extracted in the first extraction step with dithionite-bicarbonate (0.1 µM, 8h, 20°C). Na-
185 acetate buffer (1 µM, pH=4, 6h, 20°C) followed by $MgCl_2$ wash (1 µM, pH=8, 0.5h, 20°C) were
186 then used to recover authigenic P (carbonate fluoroapatite $Ca_5(PO_4,CO_3)_3F$, biogenic
187 hydroxyapatite $Ca_{10}(PO_4)_6(OH)_2$, $CaCO_3$-bound P) noted Aut-P (step 2). The detrital

188 fluoroapatite-bound P (Det-P) was determined in a third step of HCl (1 µM) overnight. Organic P
189 (Orga-P) was finally determined by ashing at 550 °C for 4h and using HCl (1 µM) overnight
190 (step 4).

191 PO_4^{3-}, NH_4^+ and (NO_3^- + NO_2^-) concentrations were analyzed using segmented flow
192 analysis (SFA; Aminot et al., 2009) and $Si(OH)_4$ concentrations were determined with an
193 AutoAnalyzer III (Bran+Luebbe®) using the method of Tréguer and Le Corre (1975). Fe^{2+}
194 concentrations were measured with the ferrozine method (Sarradin et al. 2005) and Mn^{2+} with the
195 leuco-malachite green method (Resing and Mottl 1992), both adapted for SFA. The precision of
196 the analyses was 0.5 %.

197

198 2.4. Data processings

199

200 Pictures of longitudinal sections were obtained in dicom format to be later analyzed by
201 image J® software. We analyzed the sedimentary structure of each core by using a tomogram
202 representing tomographic intensities (TI) expressed in Hounsfield units (HU) along a longitudinal
203 plane for the entire length of the core (Gagnoud et al. 2009; Michaud et al. 2003). The calibration
204 gave specific values for tomographic intensities according to analyzed materials (i.e., TI_{air} = -
205 1000; TI_{water} = 0; $TI_{calcite}$ = 2500). To simplify illustrations, picture and TI profile are presented for
206 only one core because of the low variability of duplicates. Duplicate variability was studied in
207 February and July at stations A2 and A3. At each sediment depth, the variability was very low in

the outer estuary (CV[‡] < 10%) and slightly higher in the mid estuary (CV < 20%). Higher heterogeneity between duplicates was only locally observed below 5 cm depth, with CV reaching a maximum of 50 % at A3 and 60-80 % at A2 at some local depths. This local heterogeneity in deep sediment layers was mostly explained by the presence of a rock or bioturbation in the outer estuary, and by a small vertical shift of deep layers between duplicates in the mid estuary because of the sloping core layers. Except these local and deep heterogeneities, the general form of TI profiles was similar between duplicates. This confirms that the analysis of one core is enough to highlight the sedimentary facies at each station.

Surfer® software was used to interpolate measured values year round and create contour maps for P form concentrations, dissolved species concentrations, and dissolved species molar ratios (i.e., NH_4^+:PO_4^{3-} and Fe^{2+}:PO_4^{3-} ratios).

All statistical analyses were performed with R software (http://cran.r-project.org). The normality and homoscedasticity of data sets were first assessed with Shapiro and Bartlett tests to determine the suitability of these data sets for parametric or non-parametric statistical tests. Wilcoxon or *t*-tests were performed to determine significant differences of porosity and grain size between stations or seasons. Pearson or Spearman correlations were used to evaluate relationships between all measured variables (Orga-P, Fe-P, Aut-P, Det-P, PO_4^{3-}, NH_4^+, (NO_3^- + NO_2^-), $Si(OH)_4$, Fe^{2+}, Mn^{2+}, porosity). For all tests, values were considered significant at $p < 0.05$.

[‡] CV is the coefficient of variation e.g. the standard deviation as a percentage of the mean

3. Results

3.1. Surface sediment grain size

Even not significant (Table 2), the proportion of fine sediments (% < 63 μm) in surface sediments was slightly lower in February (78 ± 6 %) than during other seasons (82 ± 3 %; Table 1) in the inner estuary (station A1). The proportion of fine surface sediments was lower in the intermediate estuary (station A2; 37-64 %) than at stations A1 and A3 (> 70 %; Table 1).

3.2. Porosity and salinity

In the inner estuary (station A1), porosity in surface sediments was significantly lower in February (0.82; Fig. 3, A1) compared to other months (> 0.9; Table 2). The porosity decreased with depth from 0.82 to 0.75 in February and from 0.95 to 0.8 in May, July and October. The intermediate estuary (station A2) showed a particular pattern with layers of low (0.65-0.75) and high porosity (0.8-0.9) alternated along the core in February, July and October (Fig. 3, A2), but profiles decreasing progressively over depth in May (0.88 to 0.6). In the outer estuary (station A3), the porosity decreased with depth from 0.88 to 0.76 except some local discontinuities in July and October (Fig. 3, A3). Contrary to the vertical decrease in porosity, pore water salinity was constant over depth in May or very slightly increased along each core in February (analyses not

248 performed in July and October), and increased from station A1 to station A3 (Khalil et al.
249 submitted).

250

251 3.3. Tomographic intensity

252

253 In the inner estuary, the tomogram indicated two different levels of TI in February and
254 July (Fig. 3, A1). A layer of low density sediments (TI < 400 HU), corresponding to fluid muds
255 observed during core samplings, was pointed out at 0-3 cm depth in February and at 0-15 cm
256 depth in July, while more dense sediments (TI = 700 HU) were observed deeper. Homogeneous
257 TI values (350-450 HU) were measured over depth in October, when fluid muds were observed
258 throughout whole cores.

259 In the mid estuary, TI values varied over a large range over depth (200 to > 1100 HU; Fig.
260 3, A2). In February, the lowest density (< 400 HU) was measured at 0-2 cm, while the highest
261 and very variable density (600 to 1100 HU) was observed at 3-20 cm. Two thick bands of white
262 color on the CAT scan pictures indicated particularly dense deposits (1100 HU) at 12 and 14 cm
263 depth. These dense deposits (>1100 HU) were found at 6 and 8 cm depth in July. They were
264 separated by relatively soft deposits (TI ~ 200 HU; plant detritus observed during core slicing).
265 More (800 HU) and less (200-500 HU) dense deposits alternated every 1 or 2 cm at 0-15 cm.
266 Below 15 cm depth, the TI range was smaller (500 to 800 HU). In October, we observed the same
267 pattern as in July. The same dense deposits (TI value > 1000 HU) were observed at 0-2, 6 and 8
268 cm depth. These dense layers were still separated by very soft sediments (200 HU) at 4, 7, and 9

cm depth.

In the outer estuary, deposit properties were less variable over depth (500-800 HU) than in the mid estuary, but varied over the seasons (Fig. 3, A3). In February, the density of deposits averaged at 500 HU, whereas four layers of denser deposits (800 HU) appeared at 10, 12, 16 and 20 cm depth. In July, the same dense deposits (800 HU) were observed 2-3 cm deeper and a new layer of dense sediments appeared at 10 cm depth. In October, the same dense deposits occurred 3-4 cm deeper than in July (at 16, 18, 22 and 26 cm depth) and a new layer of dense sediments appeared at 10 cm depth (800 HU).

3.4. Particulate P forms

In the inner estuary (station A1), maximal Orga-P concentrations occurred in surface sediment in July (up to 15.6 µmol g^{-1}; Fig. 4, A1). Orga-P concentrations generally decreased with depth, with the lowest concentrations occurring in February and October (< 6 µmol g^{-1}). Fe-P profiles showed a relatively similar pattern as those of Orga-P. The lowest concentrations occurred in depth in February and October (about 13-15 µmol g^{-1}) and coincided with Aut-P maximal concentrations (16-18 µmol g^{-1}). Low concentrations and seasonal variations of Det-P were observed (5.4 ± 1.1 µmol g^{-1}).

The mid estuary (station A2) was characterized by a vertical succession of Orga-P poor and rich layers with two marked gaps (< 1 µmol g^{-1}) in May (6-12 cm) and October (8-20 cm; Fig. 4, A2). As observed in the inner estuary, these low Orga-P concentrations in February and

290 May were observed with the lowest Fe-P concentrations (< 8 µmol g^{-1}) and the highest Aut-P
291 concentrations. In October, low Orga-P concentrations coincided however with the highest Fe-P
292 and Aut-P concentrations. Det-P concentrations generally increased with depth and from
293 February to October.

294 The outer estuary (station A3) showed relatively little seasonal variations regarding the
295 vertical profiles of phosphorus forms. Orga-P and Fe-P concentrations decreased with depth (Fig.
296 4, A3), whereas Aut-P and Det-P concentrations varied little over depth (annual and vertical
297 average concentrations of Aut-P = 6.9 ± 1.6 µmol g^{-1} and Det-P = 5.4 ± 1.1 µmol g^{-1}).

298

299 3.5. Dissolved chemical species

300

301 At all stations, the oxygen penetration depth varied from 0.5 mm to 5 mm (Khalil et al.
302 submitted). The limit between suboxic (0.2-0.0 mg L^{-1}) and anoxic (0.0 mg L^{-1}) conditions -
303 according to the classification of Tyson and Pearson (1991) - was thus always reached within the
304 first 5 mm. All pore water NO_3^- profiles showed a strong decrease of concentrations with depth
305 (Fig. 5). At all stations, NO_3^- was below the detection limit at a depth of 2-4 cm. The lowest
306 penetration depths were observed in May (A1) or in July (A2, A3).

307 In the inner estuary, pore water PO_4^{3-} concentrations were always low (< 12.1 µM; Fig. 5,
308 A1). Pore water concentrations of NH_4^+, Mn^{2+}, Fe^{2+} and $Si(OH)_4$ increased with depth at all
309 seasons and were much higher in February and May (up to 2800, 35, 900 and 580 µM,
310 respectively). NH_4^+:PO_4^{3-} and Fe^{2+}:PO_4^{3-} ratios increased up to 300, especially in February and

311 May (Fig. 6, A1).

312 In the mid estuary, on the opposite to the inner estuary, PO_4^{3-} concentrations sharply
313 increased with depth, especially in February and July (up to 259 and 193 µM; Fig. 5, A2). NH_4^+
314 concentrations never exceeded 1000 µM and decreased from February to October. Mn^{2+}, Fe^{2+} and
315 $Si(OH)_4$ were characterized by very high concentrations in subsurface sediment in February and
316 May (550-800, 1500-3000 and 28-60 µM, respectively). NH_4^+:PO_4^{3-} ratios were higher than 16 in
317 surface layers in February and in deepest layers in May but never reached the high values
318 observed at A1 (Fig. 6, A2). The highest Fe^{2+}:PO_4^{3-} ratios occurred in May but never exceeded
319 70.

320 In the outer estuary, dissolved species showed vertical distributions observed typically for
321 sediments undergoing diagenesis. PO_4^{3-}, NH_4^+ and $Si(OH)_4$ concentrations increased with depth,
322 while Mn^{2+} and Fe^{2+} showed maximal subsurface concentrations (Fig. 5, A3) . The deepest part
323 of the sediment core contained the highest PO_4^{3-} concentrations in May, and the highest NH_4^+ and
324 $Si(OH)_4$ concentrations in July. Mn^{2+} and Fe^{2+} showed maximal subsurface concentrations never
325 exceeding 252 µM and 42 µM, respectively, in October. On the opposite to the inner estuary,
326 NH_4^+:PO_4^{3-} and Fe^{2+}:PO_4^{3-} ratios rarely exceeded values of 16 and 2, respectively, and decreased
327 over depth (Fig. 6, A3).

328

329 3.6. Correlations between benthic properties

330

331 Pearson correlations were calculated on the matrix of measured variables (Table 3). In the

inner and outer estuary (stations A1 and A3), Orga-P was positively correlated to (NO_3^- + NO_2^-), Fe-P and porosity, and negatively correlated to $Si(OH)_4$, NH_4^+, Mn^{2+} and Det-P. In the mid and outer estuary (stations A2 and A3), positive correlations were observed for $Si(OH)_4$ *vs* PO_4^{3-}, $Si(OH)_4$ *vs* NH_4^+, and PO_4^{3-} *vs* NH_4^+. Negative correlations of Orga-P with PO_4^{3-} and Aut-P were only found in the inner estuary. At this station (A1), positive correlations were observed between $Si(OH)_4$, NH_4^+, Fe^{2+}, Mn^{2+} and Det-P *vs* Aut-P, while negative correlations were observed for PO_4^{3-}, Fe-P and Orga-P *vs* Aut-P, and NH_4^+ and $Si(OH)_4$ *vs* PO_4^{3-}. In the mid estuary, Aut-P was positively correlated with Fe-P, and negatively correlated with Aut-P.

4. Discussion

Enhancement of benthic biogeochemical processes in inner estuary

The inner estuary is characterized by the presence of fluid muds (Fig. 3, A1). This estuarine feature is commonly observed at water salinity ranging between 0 and 10 due to suspended matter flocculation, sedimentation, upward transport by residual bottom currents, and tidal asymmetry (Allen et al. 1980; Postma 1967; Woodruff et al. 2001). The increase of fluid mud thickness over the year - from ~ 2 cm in February to 15 cm in July and > 20 cm in October (Fig. 3) - is associated to the river discharge decrease (Fig. 2) and the progressive accumulation of sediments in the inner Aulne Estuary (Bassoulet 1979). The seasonal increase of the fluid mud thickness leads to seasonal variations of vertical profiles of porosity and particulate and dissolved

353 species (Figs. 3, 4 and 5) which are correlated (Table 3), especially Fe-P and Orga-P. The high
354 Fe-P concentrations in fluid muds highlight the potential stocks of quickly available P due to the
355 sorption of P onto sediments (Mayer and Gloss 1980). The high Orga-P concentrations show that
356 fluid muds are also enriched in organic matter. These results are consistent with the general
357 description of fluid muds that are considered as reactors for intense organic matter recycling
358 (Aller 2004).

359 The high pore water NH_4^+, Mn^{2+}, Fe^{2+} and $Si(OH)_4$ concentrations in the inner estuary in
360 February indicate (1) the high benthic mineralization resulting from the high loads of organic and
361 silicified matter associated to fluid muds, (2) the sediment re-oxidation after erosion, and (3) the
362 presence of older sediments. High pore water concentrations of NH_4^+, Mn^{2+} and Fe^{2+} (Fig. 5, A1)
363 and low oxygen penetration depth (< 5 mm; Khalil et al. submitted) in the inner estuary in winter,
364 when fluid muds are absent, highlight intense organic matter degradation mediated by bacteria
365 (Berner 1980; Soetaert et al. 1998), thus leading to the vertical decrease of Orga-P concentrations
366 (Fig. 4, A1). Even if fluid muds are absent in winter (during the short period of higher river
367 discharge), organic matter is brought year-round by the accumulation of fluid muds in the inner
368 estuary, which increase benthic mineralization processes. High pore water $Si(OH)_4$
369 concentrations in the inner estuary indicate that amorphous Si is associated with this organic
370 matter and characterized by intense benthic dissolution (Berner 1980). This load of amorphous Si
371 was confirmed by the high amorphous Si concentrations observed in the Aulne surface freshwater
372 in February (Raimonet et al. 2013). Additionally, the high discharge of river waters enriched with
373 O_2 and NO_3^- lead to an increase of (NO_3^- + NO_2^-) concentration and penetration in surface
374 sediments. The enhanced penetration depth of highly oxidative O_2 and NO_3^- in February then

intensifies mineralization processes (Berner 1980), anaerobic reduced metabolite re-oxidation (Aller et al. 2004) and decreases the use of other electron acceptors. Increasing Mn^{2+} and Fe^{2+} concentrations and decreasing Fe-P concentrations over depth suggest that Mn and Fe oxides facilitate mineralization down to (NO_3^- + NO_2^-) penetration depth in sediment. These high concentrations of NH_4^+, Mn^{2+}, Fe^{2+} and $Si(OH)_4$ (Fig. 5, A1) and the vertical decrease in Orga-P and Fe-P concentrations which are particularly high in surface layers (Fig. 4, A1) highlight thus the high mineralization activity of re-oxidized sediments after fluid mud displacement, which has already been observed in the Amazon Shelf (Aller 2004). Finally, the erosion of fluid muds exposes older and more compact sediments, which were similar by low % < 63 µm (and porosity, this study) to sediments collected in the Seine and Palmones estuaries after flooding events (Lesourd et al. 2003; Avilés and Niell 2005). The presence of reducing conditions in the old exposed sediments in the inner estuary, in association with higher initial P-bearing components (Orga-P and Fe-P) and lower salinity compared to the mid and outer estuary, might have enhanced the precipitation of Aut-P (detailed below), as all these conditions are favorable for Aut-P precipitation (Ruttenberg and Berner 1993; Slomp et al. 1996).

The precipitation of Aut-P in sediment is highlighted by NH_4^+: PO_4^{3-} and Fe^{2+}: PO_4^{3-} ratios much higher than 16 and 2, respectively (Fig. 6). High NH_4^+: PO_4^{3-} ratios indicate that mineralization alone cannot explain the vertical profiles of dissolved species, and that NH_4^+ formation and/or PO_4^{3-} removal may take place in these sediments (Ruttenberg and Berner 1993). Even if NH_4^+ might have formed from dissimilatory NO_3^- reduction to NH_4^+ (DNRA) (Laverman et al. 2006; Gardner and McCarthy 2009), the production of NH_4^+ would have not led to such high NH_4^+: PO_4^{3-} ratios in the inner estuary in February. Moreover, Fe^{2+}: PO_4^{3-} ratios would have

been close to the theoretical ratio of 2 iron oxyhydroxide molecules linked to each $H_2PO_4^-$ ion (Lijklema 1977; Lehtoranta and Heiskanen 2003). In our study, the high Fe^{2+}: PO_4^{3-} ratios (Fig. 6) indicate Fe^{2+} release during Fe oxide reduction, and PO_4^{3-} removal through precipitation. These simultaneously high NH_4^+: PO_4^{3-} and Fe^{2+}: PO_4^{3-} ratios - previously reported for freshwater sediments (Hartzell et al. 2010) -, and the low PO_4^{3-} concentrations (< 5 µM) are consistent with the presence of Aut-P (Slomp et al. 1996), confirming that Aut-P precipitation happened (Berner 1980).

Precipitation of Aut-P generally results from the removal of free PO_4^{3-} in pore waters, issued from Fe-P dissolution and from Orga-P mineralization in anoxic conditions (Ruttenberg and Berner 1993; Reimers et al. 1996; Slomp et al. 1996). In this study, the negative correlations of Fe-P and Orga-P *vs* Aut-P (Table 3), and the vertical decrease of Fe-P concentrations (Fig. 7) in the inner estuary indicate that Aut-P precipitates from PO_4^{3-} originated from both Orga-P and Fe-P. Such high Aut-P concentrations (> 14 µmol g^{-1}) have never been observed in other systems (Table 4). The intense precipitation of Aut-P in the inner estuary results of the presence of reducing conditions in older sediments, which conditions are known to increase the preservation of P (Jilbert et al. 2011) and thus Aut-P precipitation (Slomp et al. 1996). The presence of lower pH, sulfate and Mg^{2+} concentrations in fresh compared to marine waters also favors the formation of Aut-P by limiting the competition of PO_4^{3-} with OH^- and sulfate for sorption sites, and the competition of Mg^{2+} with Ca^{2+} (Caraco et al. 1989; Mayer and Jarrell 2000; Gunnars et al. 2004; Hyacinthe and Van Cappellen 2004). Other factors - that have been shown to potentially constrain sorption processes along estuaries, in laboratory conditions - are also expected to influence the precipitation of Aut-P, e.g. specific surface area and mineral composition of

419 particles, cation exchange capacity, bacterial uptake, presence of arsenate, organic, humic or
420 fulvic acids (Fontes and Weed 1996; Sundareshwar and Morris 1999; Violante et al. 2002; Cao et
421 al. 2007; Loucaides et al. 2010). More studies are however needed to investigate the role of these
422 factors in estuarine environments.

423 As the formation of Fe-P was reported to be highly increased in the presence of $Si(OH)_4$
424 that leads to Si-enriched Fe oxides, especially at low pH (Mayer and Jarrell 2000), we also
425 explored the indirect role of high $Si(OH)_4$ concentrations in the precipitation of Aut-P in inner
426 estuary where the freshwater is more Si-enriched and acid than marine waters. In this study,
427 $Si(OH)_4$ concentrations associated with high Aut-P concentrations reach more than 400 µM in the
428 inner estuary in February. We hypothesize that high $Si(OH)_4$ concentrations increase first Fe-P
429 formation during Fe oxidation in surface sediments, which is known to favor Aut-P formation
430 (Slomp et al. 1996). In the deepest anoxic sediments, high $Si(OH)_4$ concentrations saturate
431 mineral sorption sites, and thus release free PO_4^{3-} (Mayer and Jarrell 2000). High free PO_4^{3-}
432 concentrations mediated by high $Si(OH)_4$ concentrations favor then Aut-P formation observed in
433 these same layers. The high $Si(OH)_4$ concentrations suggest that continuous and high dissolution
434 of Si-enriched Fe oxides happen in deep sediments. Even if high $Si(OH)_4$ concentrations and
435 resuspension events were shown to potentially enhance benthic fluxes of PO_4^{3-} (Tallberg et al.
436 2008; de Vicente et al. 2010), the present study also suggests that these conditions could
437 indirectly increase Aut-P precipitation in low salinity waters.

438 Additionally to these numerous favorable conditions for Aut-P precipitation in inner
439 estuarine sediments, Aut-P might have also been partly brought by upper riverine freshwaters.
440 Aut-P concentrations in surface sediments reached up to 11 µmol g^{-1} which can attest of erosion

of surface Aut-P poor sediments and/or of loads of allochthonous riverine Aut-P. Aut-P indeed preferentially precipitates in freshwater environmental conditions i.e. low pH, sulfate and Mg^{2+} concentrations (see above). The decrease of surface Aut-P concentrations towards the outer estuary indicates the dilution and the settlement of Aut-P along the estuary. The higher Aut-P contents in the inner estuary thus results from a combination of reducing conditions, high loads of Orga-P, Fe-P and Aut-P, and the presence of freshwaters (low pH, OH^-, sulfate and Mg^{2+} concentrations, high $Si(OH)_4$ concentrations).

Regardless of the factors leading to Aut-P precipitation, the formation of Aut-P both (1) decreases PO_4^{3-} fluxes, and (2) increases P retention. The trapping of PO_4^{3-} through Aut-P precipitation might indeed decrease benthic fluxes of PO_4^{3-} to the water column, which means that benthic fluxes may have even been higher if PO_4^{3-} reprecipitation into Aut-P had not occurred. Aut-P forms - which have a higher potential of long term sinking in comparison with the more reactive P forms - also contribute to an efficient storage of P in benthic sediments (Ruttenberg and Berner 1993). The contribution of Aut-P formation in P storage in the inner Aulne Estuary ranges between 24 and 36 % of total P forms regardless of the season (not shown), agreeing with the high values (28 to 50 %) reported previously (Ruttenberg and Berner 1993; Andrieux and Aminot 1997), and suggesting high potential for long term P storage in the inner estuarine sediments.

Role of point bar hydrodynamics in modulating the benthic biogeochemistry in the mid-estuary

463 The succession of sediment layers highlights the turbulent hydrodynamic conditions (e.g.
464 bottom currents, tides) in mid estuarine point bars. Turbulent hydrodynamic conditions in
465 estuaries are generally associated to low concentrations of clay, organic matter and chlorophyll a
466 (Moreno and Niell 2004). In our study, the low clay and silt contents and the generally lower
467 Orga-P than Det-P concentrations in the mid estuary confirm highly dynamic conditions. The
468 vertically heterogeneous sediment tomographic intensity observed in CAT scan cores (Fig. 3, A2)
469 and the succession of muddy and detrital sediments (described above) moreover indicate the
470 variability of dynamic conditions over time in the mid estuary, where the highest tidal energy
471 occurs (Dyer 1989). Related to intense erosion-deposition events, the vertical heterogeneity in
472 sediment cores was also observed along and across the mid estuary through an extensive
473 investigation of spatial heterogeneity of pore water $Si(OH)_4$ profiles (Raimonet et al. 2013). High
474 heterogeneity in sediments from the mid Aulne Estuary is expected and consistent with the
475 highest variability observed in the mid Palmones and Penzé estuaries (Avilés and Niell 2005;
476 Andrieux-Loyer et al. 2008) resulting from the hydrodynamic regime (Dyer 1989).
477 Contrary to the inner estuary, Aut-P concentrations do not increase with depth in the mid
478 estuary but are associated to a succession of poor and enriched layers (Fig. 4), consistent with the
479 presence of less and highly dense sediments (Fig. 3). The succession of layers of different
480 properties suggests that the properties of sediment loads vary over time, each layer corresponding
481 to different periods and origins. The Aut-P enriched layers suggest the translocation and
482 deposition of freshwater or less marine sediments, as Aut-P preferentially precipitates in
483 freshwater environmental conditions (as detailed above). The Aut-P present in subsurface
484 sediment layers might have been formed upstream, e.g. in the river or the inner estuary, and then

485 transported to the mid estuary. The presence of high Mn^{2+}, Fe^{2+} and $Si(OH)_4$ concentrations in
486 these same Aut-P enriched layers confirms that this translocation from the inner to the mid
487 estuary might happen.

488 The high Mn^{2+} and Fe^{2+} concentrations, associated to high $Si(OH)_4$ concentrations in
489 subsurface layers in February and May in the mid-estuary (Fig. 5, A2), also highlight the
490 presence of detrital terrestrial materials in deposits. The co-occurrence of these high
491 concentrations might indeed result from the dissolution of the generally high Fe and Mn oxide
492 concentrations associated with detrital terrestrial materials (Aller et al. 2004). These layers might
493 result from the deposition of the terrestrial plant material exported from river and estuarine
494 borders to estuarine waters (Bassoulet 1979), which commonly happen in temperate macrotidal
495 estuaries during winter (Anderson et al. 1981). The export of silicified plants growing in
496 estuarine marshes - mainly *Phragmites australis* in the Aulne Estuary - is known to be high after
497 the high productive period in fall and during the high winter river discharge (Findlay et al. 1990;
498 Querné 2011). This is consistent with the export of Si enriched materials and the high amorphous
499 Si concentrations observed in February in the upper estuary (80 µM; Raimonet et al. 2013). A
500 part of this exported matter may settle in mid estuarine point bars. It is however difficult to go
501 further on the correspondence between layers and matter origin, because of the erosion-
502 deposition cycles that perturb the vertical sequence.

503 The vertical profiles of particulate and dissolved matter and the scan images allow,
504 however, estimating net seasonal deposition and erosion rates. The temporal deepening of the
505 maximal subsurface Mn^{2+}, Fe^{2+} and $Si(OH)_4$ concentrations (observed at 1-4 cm in February, and
506 at 2-7 cm in May; Fig. 5, A2) suggests the deposition of ~ 1-3 cm of sediment between February

and May. TI and CAT scan cores also show that sediment erosion happens between May and July (Fig. 3, A2). After erosion, older sediments - that were initially deeper - are exposed to pelagic waters. In contrast to the inner estuary (A1) where the downward displacement of fluid muds in February leads to high NH_4^+, Mn^{2+}, Fe^{2+} and $Si(OH)_4$ concentrations, sediments in the mid estuary have lower concentrations after erosion. These lower concentrations in mid compared to inner estuarine sediments after erosion are related to the presence of coarser sediments associated to lower porosity and lower organic matter content (e.g. Orga-P concentrations; Fig. 4, A2) due to more turbulent hydrodynamic conditions.

Such as in the inner estuary, evidence of *in situ* Aut-P precipitation in the mid Aulne Estuary is indicated by NH_4^+: PO_4^{3-} and Fe^{2+}: PO_4^{3-} ratios higher than 16 and 2, respectively (Fig. 6, A2), and by the negative correlation between Aut-P and Orga-P (Table 3). Vertically stable Fe-P concentrations in the mid estuary in October indicate that PO_4^{3-} leading to high Aut-P concentrations is not originated from Fe-P dissolution, but rather from Orga-P oxidation in the mid estuary (mirror profiles of Orga-P and Aut-P; Fig. 7). The decrease of NH_4^+: PO_4^{3-} down to 12 cm emphasizes that the remineralization of P relative to N increases with depth, consistent with the increasingly reductive conditions (Jilbert et al. 2011). As the effect of high $Si(OH)_4$ concentrations on the benthic P cycle is mainly mediated through the increased formation of Fe-P, the preferential origins of Aut-P from Orga-P indicate that the interactions between Si and P cycles may be low in the mid estuary.

Marine-type benthic biogeochemistry in the outer estuary

529 Continuous deposition of sediments takes place throughout the year in the outer estuary.
530 The net deposition rate is high (2-3 cm) from February to July and even higher (~ 4 cm) from
531 July to October (Fig. 3). Lower hydrodynamic energy - explaining high deposition rates - leads to
532 classical diagenetic profiles and low seasonal variability for solid and dissolved species in the
533 outer estuary. During the productive period in May, chlorophyll a concentrations were higher
534 (Raimonet 2011), and expectedly related to the occurrence of the maximal Orga-P concentrations
535 in surface sediments, and the vertical decrease of Orga-P and Fe-P concentrations. In contrast to
536 the inner and mid estuary, the lowest Orga-P concentrations measured in the outer estuary may
537 also be related to the presence of bioturbation at this station (pers. obs.) - known to enhance
538 organic matter degradation (Aller 1994) and to the higher degradability of marine compared to
539 terrestrial organic matter. High PO_4^{3-} and low Fe-P concentrations may be due to the proximity of
540 oceanic waters in the outer estuary. Indeed, the presence of sulfate-rich marine waters commonly
541 leads to the formation of Fe sulfides in anoxic conditions, limiting Fe-P formation (Caraco et al.
542 1989; Hyacinthe and Van Cappellen 2004). As excepted, the increase in NH_4^+ concentrations
543 from the inner to the outer estuary in May, July and October may also be related to increasing
544 salinity known to enhance NH_4^+ desorption from particles (Hartzell et al. 2010).

545 NH_4^+: PO_4^{3-} ratios are expected to be close to the Redfield ratio (16) in conditions of
546 organic matter regeneration. The NH_4^+: PO_4^{3-} ratios < 16 (this study) provides evidence of Fe-P
547 dissolution, as already shown in the Baltic Sea (Jilbert et al. 2011). This is confirmed by
548 decreasing Fe-P and increasing PO_4^{3-} profiles. The general enhancement of pH and OH^-
549 concentrations from inner to outer estuaries (http://www.donnees.bretagne.developpement-
550 durable.gouv.fr), the high pore water $Si(OH)_4$ concentrations (Fig. 5, A3) and the sulfate-enriched

551 marine waters are indeed expected to increase PO_4^{3-} desorption (Caraco et al. 1989; Mayer and
552 Jarell 2000; Hyacinthe and Van Cappellen 2004). In spite of high pore water PO_4^{3-}
553 concentrations, Aut-P concentrations are generally lower (< 10 µmol g^{-1}) in the outer than in the
554 inner and mid estuary, in particular in February and May. The precipitation to Aut-P is rather
555 limited by the low Orga-P and Fe-P concentrations (Fig. 4, A3) and the high Mg^{2+} concentrations
556 of marine waters that compete with Ca^{2+} in outer brackish estuaries (Gunnars et al. 2004; Cao et
557 al. 2007).

558

559 ## 5. Conclusion

560

561 We highlight the influence of a combination of factors on benthic biogeochemical
562 processes along a salinity gradient in a small macrotidal estuary. These results emphasize that P
563 retention might be important in freshwater estuaries, due to favorable conditions to the
564 precipitation of low reactive Aut-P (i.e. high organic and iron-bound P loads, anoxic conditions,
565 low pH, sulfate and Mg^{2+} concentrations) and to the settlement of riverine P. In these freshwater
566 conditions, we suggest that Aut-P precipitation could be additionally enhanced in Si-rich
567 sediments by increasing the formation of Fe-P, a precursor of Aut-P. More studies are however
568 needed to highlight that interactions between Si and P cycles could have a significant role in the
569 long term storage of P. In the mid estuary, frequent erosion-deposition events, including
570 translocation, lead to a succession of heterogeneous sediment layers and biogeochemical
571 properties in point bar. More studies are needed to define seasonal origins of the deposited

matter, and erosion-deposition dynamics in point bars. Contrary to the inner and mid estuary, the outer estuary is representative of less perturbed and more marine ecosystems. This study emphasizes the strong estuarine gradient of benthic biogeochemical properties, and especially the long term storage of P in inner estuaries and high benthic stocks (and thus fluxes) of dissolved species, especially NH_4^+ and $Si(OH)_4$, which have important implications for coastal ecosystems, and should be accounted for in ecological studies.

Acknowledgements

This work was supported by the French National Program for Coastal Environment (PNEC-EC2CO), the Conseil Général du Finistère and the Ministère de l'Enseignement Supérieur et de la Recherche. We gratefully thank the R/V Côtes de la Manche crew, Manon Le Goff, Agnès Youenou, Christophe Rabouille, Bruno Bombled and Julien Queré for their valuable aid for cores sampling and processing, Erwan Amice and Robert Marc for their helpfull assistance on board the *Hésione* (IUEM), Eric Legoff, Nicole Gouriou and Elisabeth Bruyant for their assistance at the hospital, Monique Briand for her help with figures, and Zosia Baumann for her language edition advices. We sincerely thank two reviewers and especially Tom Jilbert for his insightful critical comments and suggestions.

589 *References*

590

591 Allen GP, Salomon JC, Bassoullet P, Du Penhoat Y, de Grandpré C (1980) Effects of tides on
592 mixing and suspended sediment transport in macrotidal estuaries. Sediment. Geol. 26(1-3):69-90
593 Aller RC (1994) Bioturbation and remineralization of sedimentary organic matter: effects of
594 redox oscillation. Chem. Geol. 114(3-4):331-345
595 Aller RC (2004) Conceptual models of early diagenetic processes: The muddy seafloor as an
596 unsteady, batch reactor. J. Mar. Res. 62:815-835
597 Aller RC, Mackin JE, Ullman WJ, Chen-Hou W, Shing-Min T, Jian-Cai J, Yong-Nian S, Jia-
598 Zhen H (1985) Early chemical diagenesis, sediment-water solute exchange, and storage of
599 reactive organic matter near the mouth of the Changjiang, East China Sea. Cont. Shelf Res.
600 4(1/2):227-251
601 Aller RC, Heilbrun C, Panzeca C, Zhu Z, Baltzer F (2004) Coupling between sedimentary
602 dynamics, early diagenetic processes, and biogeochemical cycling in the Amazon–Guianas
603 mobile mud belt: coastal French Guiana. Mar. Geol. 208:331-360
604 Aminot A, Kérouel R, Coverly SC (2009). Nutrients in seawater using segmented flow analysis.
605 In: Wurl O (ed.) Practical guidelines for the analysis of seawater. CRC Press, Boca Raton, USA,
606 pp 143-178
607 Anderson FE, Black L, Watling LE, Mook W, Mayer LM (1981) A temporal and spatial study of
608 mudflat erosion and deposition. J. Sediment. Res. 51:729-736
609 Andrieux F, Aminot A (1997) A two-year survey of phosphorus speciation in the sediments of
610 the Bay of Seine (France). Cont. Shelf Res. 17:1229-1245

611 Andrieux-Loyer F, Philippon X, Bally G, Kérouel R, Youenou A, Le Grand J (2008) Phosphorus
612 dynamics and bioavailability in sediments of the Penzé Estuary (NW France): in relation to
613 annual P-fluxes and occurrences of *Alexandrium Minutum*. Biogeochemistry 88(3):213-231
614 Anschutz P, Zhong S, Sundby B, Mucci A, Gobeil C (1998) Burial efficiency of phosphorus and
615 the geochemistry of iron in continental margin sediments. Limnol. Oceanogr. 43(1):53-64
616 Aspila KI, Agemian H, Chau ASY (1976) A semi-automated method for the determination of
617 inorganic, organic and total phosphate in sediments. The Analyst 101(1200):187-197
618 Avilés A, Niell FX (2005) Pattern of phosphorus forms in a Mediterranean shallow estuary:
619 Effects of flooding events. Estuar. Coast. Shelf Sci. 64(4):786-794
620 Bassoulet P (1979) Etude de la dynamique des sédiments en suspension dans l'estuaire de l'Aulne
621 (rade de Brest). Ph.D. Thesis, Université de Bretagne Occidentale, Brest, France, 136 pp
622 Berner RA (1980) Early diagenesis: a theoretical approach. Princeton University Press
623 Berner RA, Rao JL (1993) Phosphorus in sediments of the Amazon River and estuary:
624 Implications for the global flux of phosphorus to the sea. Geochim. Cosmochim. Acta
625 58(10):2333-2339
626 Beucher C, Treguer P, Corvaisier R, Hapette AM, Elskens M (2004) Production and dissolution
627 of biosilica, and changing microphytoplankton dominance in the Bay of Brest (France). Mar.
628 Ecol. Prog. Ser. 267:57-69
629 Cao X, Harris WG, Josan MS, Nair VD (2007) Inhibition of calcium phosphate precipitation
630 under environmentally-relevant conditions. Sci. Tot. Environ. 383:205-215
631 Caraco NF, Cole JJ, Likens GE (1989) Evidence for sulfate-controled phosphorus release from
632 sediments of aquatic systems. Nature 341:316-318

633 Cloern JE (2001) Our evolving conceptual model of the coastal eutrophication problem. Mar.
634 Ecol. Prog. Ser. 210:223-253
635 Conley DJ (2000) Biogeochemical nutrient cycles and nutrient management strategies.
636 Hydrobiol. 410:87–96
637 Conley DJ, Schelske CL, Stoermer EF (1993) Modification of the biogeochemical cycle of silica
638 with eutrophication. Mar. Ecol. Prog. Ser. 101:179-192
639 Day JW (1989) Estuarine ecology. Wiley-Interscience
640 De Montety L, Long B, Desrosiers G, Crémer J-F, Locat J, Stora G (2003) Utilisation de la
641 scanographie pour l'étude des sédiments : influence des paramètres physiques, chimiques et
642 biologiques sur la mesure des intensités tomographiques. Can. J. Earth Sci. 40:937-948
643 de Vicente I, Cruz-Pizarro L, Rueda, FJ (2010). Sediment resuspension in two adjacent shallow
644 coastal lakes: controlling factors and consequences on phosphate dynamics. Aquat. Sci. 72(1):21-
645 31
646 Dyer (1989) Estuarine flow interaction with topography - Lateral and longitudinal effects in
647 Estuarine circulation. In: Neilson BJ, Kuo A, Brubaker J (ed) Estuarine circulation. Humana
648 Farmer VC, Delbos E, Miller JD (2005) The role of phytolith formation and dissolution in
649 controlling concentrations of silica in soil solutions and streams. Geoderma 127(1-2):71-79
650 Findlay S, Howe K, Austin HK (1990) Comparison of Detritus Dynamics in Two Tidal
651 Freshwater Wetlands. Ecology 71(1):288-295
652 Fontes MPF, Weed SB (1996) Phosphate adsorption by clays from Brazilian Oxisols:
653 relationships with specific surface area and mineralogy. Geoderma 72:37-51
654 Froelich PN, Arthur MA, Burnett WC, Deakin M, Hensley V, Jahnke R, Kaul L, Kim KH, Roe

K, Soutar A, Vathakanon C (1988) Early diagenesis of organic matter in Peru continental margin sediments: Phosphorite precipitation. Mar. Geol. 80(3-4):309-343

Gagnoud M, Lajeunesse P, Desrosiers G, Long B, Dufour S, Labrie J, Mermillod-Blondin F, Stora G (2009) Litho- and biofacies analysis of postglacial marine mud using CT-scanning. Engineering Geol. 103:106-111

Gardner WS, McCarthy MJ (2009) Nitrogen dynamics at the sediment–water interface in shallow, sub-tropical Florida Bay: why denitrification efficiency may decrease with increased eutrophication. Biogeochemistry 95:185-198

Gehlen M, Van Raaphorst W (2002) The role of adsorption-desorption surface reactions in controlling interstitial Si(OH)4 concentrations and enhancing Si(OH)4 turn-over in shallow shelf seas. Cont. Shelf Res. 22(10):1529-1547

Gunnars A, Blomqvist S, Martinsson C (2004) Inorganic formation of apatite in brackish seawater from the Baltic Sea: an experimental approach. Marine Chemistry 91:15-26

Hartikainen H, Pitkänen M, Kairesalo T, Tuominen L (1996) Co-occurrence and potential chemical competition of phosphorus and silicon in lake sediment. Wat. Res. 30(10):2472-247

Hartzell J, Jordan T, Cornwell J (2010) Phosphorus burial in sediments along the salinity gradient of the Patuxent River, a subestuary of the Chesapeake Bay (USA). Estuar. Coasts 33:92-106

Howarth RW, Marino R (2006) Nitrogen as the limiting nutrient for eutrophication in coastal marine ecosystems: evolving views over three decades. Limnol. Oceanogr. 51(1):364-376

Howarth R, Chan F, Conley DJ, Garnier J, Doney SC, Marino R, Billen G (2011) Coupled biogeochemical cycles: eutrophication and hypoxia in temperate estuaries and coastal marine ecosystems. Front. Ecol. Environ. 9(1):18-26

677 Hyacinthe C, Van Cappellen P (2004) An authigenic iron phosphate phase in estuarine
678 sediments: composition, formation and chemical reactivity. Mar. Chem. 91(1-4):227-251
679 Jilbert T, Slomp CP, Gustafsson BG, Boer W (2011) Beyond the Fe-P-redox connection:
680 preferential regeneration of phosphorus from organic matter as a key control on Baltic Sea
681 nutrient cycles. Biogeosciences 8:1699-1720
682 Jordan TE, Cornwell JC, Boynton WR, Anderson JT (2008) Changes in phosphorus
683 biogeochemistry along an estuarine salinity gradient: The iron conveyer belt. Limnol. Oceanogr.
684 53(1):172-184
685 Khalil K, Raimonet K, Laverman AM, Yan C, Andrieux-Loyer F, Viollier E, Deflandre E,
686 Ragueneau O, Rabouille C (submitted to Aquatic Geochemistry) Spatial and temporal variability
687 of sediment organic matter recycling in two temperate small estuaries.
688 Koski-Vähälä J, Hartikainen H, Tallberg P (2001) Phosphorus Mobilization from Various
689 Sediment Pools in Response to Increased pH and Silicate Concentration. J. Environ. Quality
690 30:546-552
691 Laruelle GG (2009) Quantifying nutrient cycling and retention in coastal waters at the global
692 scale. Ph.D. Thesis, Utrecht University, Utrecht, Netherlands, 226 pp
693 Laverman A, Van Cappellen P, van Rotterdam-Los D, Pallud C, Abell J (2006) Potential rates
694 and pathways of microbial nitrate reduction in coastal sediments. FEMS Microbiol. Ecol. 58:179-
695 192
696 Lehtoranta J, Heiskanen A-S (2003) Dissolved iron:phosphate ratio as an indicator of phosphate
697 release to oxic water of the inner and outer coastal Baltic Sea. Hydrobiologia 492(1-3):69-84
698 Lesourd S, Lesueur P, Brun-Cottan JC, Garnaud S, Poupinet N (2003) Seasonal variations in the

699 characteristics of superficial sediments in a macrotidal estuary (the Seine inlet, France). Estuar.
700 Coast. Shelf Sci. 58(1):3-16
701 Lijklema L (1977) The role of iron in the exchange of phosphorus between water and sediments.
702 In. Golterman HL (ed.) Interactions between sediments and fresh water. Proc. Int. Symp.,
703 Amsterdam, the Netherlands. 6–10 Sept. The Hague, the Netherlands, pp 313-317
704 Loucaides S, Michalopoulos P, Presti M, Koning E, Behrends T, Van Cappellen P (2010)
705 Seawater-mediated interactions between diatomaceous silica and terrigenous sediments: Results
706 from long-term incubation experiments. Chem. Geol. 270:68-79
707 Louchouarn P, Lucotte M, Duchemin E, de Vernal A (1997) Early diagenetic processes in recent
708 sediments of the Gulf of St-Lawrence: phosphorus, carbon and iron burial rates. Mar. Geol.
709 139:181-200
710 Matijević S, Bojanić N, Kušpilić G, Ninčević Gladan Z (2009) Seasonal variations of phosphorus
711 species in sediment from the middle Adriatic Sea. Environ. Earth Sci. 59:853-866
712 Mayer LM, Gloss SP (1980) Buffering of silica and phosphate in a turbid river. Limnol.
713 Oceanogr. 25(l):12-22
714 Mayer TD, Jarrell WM (2000) Phosphorus sorption during iron(II) oxidation in the presence of
715 dissolved silica. Wat. Res. 34(16):3949-3956
716 Michalopoulos P, Aller RC (2004) Early diagenesis of biogenic silica in the Amazon delta:
717 alteration, authigenic clay formation, and storage. Geochim. Cosmochim. Acta 68(5):1061-1085
718 Michaud E, Desrosiers G, Long B, de Montety L, Crémer J-F, Pelletier E, Locat J, Gilbert F,
719 Stora G (2003) Use of axial tomography to follow temporal changes of benthic communities in
720 an unstable sedimentary environment (Ha!Ha! Bay, Saguenay Fjord). J. Exp. Mar. Biol. Ecol.

721 285/286:265-282
722 Moreno S, Niell FX (2004) Scales of variability in the sediment chlorophyll content of the
723 shallow Palmones River Estuary, Spain. Estuar. Coast. Shelf Sci. 60(1):49-57
724 Nelson DM, Treguer P, Brzezinski MA, Leynaert A, Queguiner B (1995) Production and
725 dissolution of biogenic silica in the ocean: Revised global estimates, comparison with regional
726 data and relationship to biogenic sedimentation. Global Biogeochem. Cycles 9(3):359-372
727 Némery J, Garnier J (2006) Typical features of particulate phosphorus in the Seine estuary
728 (France). Hydrobiologia 588:271-290
729 Postma (1967) Sediment transport and sedimentation in the estuarine environment. In: Estuaries,
730 American association for the advancement of science. Washington, pp 158-179
731 Prastka K, Sanders R, Jickells T (1998) Has the role of estuaries as sources or sinks of dissolved
732 inorganic phosphorus changed over time? Results of a Kd study. Mar. Poll. Bull. 36(9):718-728
733 Querné J (2011) Invasion de *Spartina alterniflora* dans les marais de la rade de Brest.
734 Comportement invasif et impact sur le cycle biogéochimique du silicium. Ph.D thesis, Université
735 de Bretagne Occidentale, Brest, France, 217 pp
736 Ragueneau O, Lancelot C, Egorov V, Vervlimmeren J, Cociasu A, Déliat G, Krastev A, Daoud
737 N, Rousseau V, Popovitchev V, Brion N, Popa L, Cauwet G (2002) Biogeochemical
738 Transformations of Inorganic Nutrients in the Mixing Zone between the Danube River and the
739 North-western Black Sea. Estuar. Coast. Shelf Sci. 54(3):321-336
740 Raimonet (2011) Cycle benthique du silicium dans les estuaires : observations et modélisation à
741 différentes échelles spatio-temporelles. Ph.D. Thesis, Université de Bretagne Occidentale, Brest,
742 France, 167 pp

743 Raimonet M, Ragueneau O, Andrieux-Loyer F, Philippon X, Kerouel R, Le Goff M, Mémery L
744 (2013) Spatio-temporal variability in benthic silica cycling in two macrotidal estuaries: causes
745 and consequences for local to global studies. Estuar. Coast. Shelf Sci. 119:31-43
746 Rao JL, Berner RA (1997) Time variations of phosphorus and sources of sediments beneath the
747 Chang Jiang (Yangtze River). Mar. Geol. 139:95-108
748 Reimers CE, Ruttenberg KC, Canfield DE, Christiansen MB, Martin JB (1996) Porewater pH and
749 authigenic phases formed in the uppermost sediments of the Santa Barbara Basin. Geochim.
750 Cosmochim. Acta 60(21):4037-4057
751 Resing JA, Mottl MJ (1992) Determination of manganese in seawater using flow injection
752 analysis with on-line preconcentration and spectrophotometric detection. Anal. Chem.
753 64(22):2682-2687
754 Ruttenberg KC (1992) Development of a sequential extraction method for different forms of
755 phosphorus in marine sediments. Limnol. Oceanog. 37(7):1460-1482
756 Ruttenberg KC, Berner RA (1993) Authigenic apatite formation and burial in sediments from
757 non-upwelling, continental margin environments. Geochim. Cosmochim. Acta 57(5):991-1007
758 Sarradin P-M, Le Bris N, Le Gall C, Rodier P (2005) Fe analysis by the ferrozine method:
759 Adaptation to FIA towards in situ analysis in hydrothermal environment. Talanta 66(5):1131-
760 1138
761 Seitzinger SP, Harrison JA, Dumont E, Beusen AHW, Bouwman AF (2005) Sources and delivery
762 of carbon, nitrogen, and phosphorus to the coastal zone: An overview of Global Nutrient Export
763 from Watersheds (NEWS) models and their application. Global Biogeochem. Cycles
764 19(4):GB4S01-GB04S01

765 Sharp JH, Pennock JR, Church TM, Tramontano JM, Cifuentes LA (1984). The estuarine
766 interaction of nutrients, organics, and metals: A case study in the Delaware Estuary.
767 In: Kennedy VS (ed) The estuary as a filter. Academic Press, Orlando, pp 241-258
768 Slomp K, Epping E, Helder W, Van Raaphorst W (1996) A key role for iron-bound phosphorus
769 in authigenic apatite formation in North Atlantic continental platform sediments. J. Mar. Res.
770 54(6):1179-1205
771 Smetacek VS (1985) Role of sinking in diatom life-history cycles: ecological, evolutionary and
772 geological significance. Mar. Biol. 84(3):239-251
773 Smith SV (1984) Phosphorus versus nitrogen limitation in the marine environment. Limnol.
774 Oceanog. 29:1149-1160
775 Soetaert K, Herman PMJ, Middelburg JJ, Heip C (1998) Assessing organic matter mineralization,
776 degradability and mixing. J. Mar. Res. 56(2):519-534
777 Soetaert K, Middelburg JJ, Herman PMJ, Buis K (2000) On the coupling of benthic and pelagic
778 biogeochemical models. Earth-Sci. Rev. 51(1-4):173-201
779 Sundareshwar PV, Morris JT (1999) Phosphorus sorption characteristics of intertidal marsh
780 sediments along an estuarine salinity gradient. Limnol. Oceanog. 44(7):1693-1701
781 Sundby B, Gobeil C, Silverberg N, Mucci A (1992) The phosphorus cycle in coastal marine
782 sediments. Limnol. Oceanog. 37(6):1129-1145
783 Tallberg P, Tréguer P, Beucher C, Corvaisier R (2008) Potentially mobile pools of phosphorus
784 and silicon in sediment from the Bay of Brest: Interactions and implications for phosphorus
785 dynamics. Estuar. Coast. Shelf Sci. 76(1):85-94
786 Thibodeau B, Lehmann MF, Kowarzyk J, Mucci A, d, Gélinas Y, Gilbert D, Maranger R,

787 Alkhatib M (2010) Benthic nutrient fluxes along the Laurentian Channel: Impacts on the N
788 budget of the St. Lawrence marine system. Estuar. Coast. Shelf Sci. 90:195-205
789 Tréguer P, Le Corre, P (1975) Manuel d'analyse des sels nutritifs dans l'eau de mer: utilisation
790 de l'auto-analyseur Technicon II. Université de Bretagne Occidentale, Brest, France
791 Tuominen L, Hartikainen H, Kairesalo T, Tallberg P (1997) Increased bioavailability of sediment
792 phosphorus due to silicate enrichment. Wat. Res. 32(7):2001-2008
793 Tyson RV, Pearson TH (1991) Modern and ancient continental shelf anoxia: an overview.
794 Geological Society, London, Special Publications 58:1-24
795 Violante A, Pigna M, Ricciardella, Gianfreda (2002) Adsorption of phosphate on variable charge
796 minerals and soils as affected by organic and inorganic ligands. Dev. Soil Sci. 28(1):279-295
797 Woodruff JD, Geyer WR, Sommerfield CK, Driscoll NW (2001) Seasonal variation of sediment
798 deposition in the Hudson River estuary. Mar. Geol. 179(1-2):105-119
799 Yamada SS, D'Elia CF (1984) Silicic acid regeneration from estuarine sediment cores. Mar. Ecol.
800 Prog. Ser. 18(1-2):113-118

Tables

Table 1: Environmental parameters in the inner (A1), mid (A2) and outer (A3) Aulne Estuary in February, May, July and October 2009. General parameters are the Aulne River discharge Q, the tidal range in Brest, and the water depth D at each station. Overlying waters are characterized by temperature T, salinity S, total suspended sediment TSS, and concentrations of (NO_3^-+NO_2^-), NH_4^+, PO_4^{3-} and $Si(OH)_4$ (n=3). The grain size (% < 63 µm) of surface sediment is also given (n=3).

Station	Sampling date	Q	Tidal range	D	T	S	TSS	(NO_3^- +NO_2^-)	NH_4^+	PO_4^{3-}	Fe^{2+}	Mn^{2+}	$Si(OH)_4$	< 63 µm
		($m^3 s^{-1}$)	(m)	(m)	(°C)	(-)	(mg l^{-1})	(µM)						(%)
A1	14/02/2009	64.6	5.2	2.5	7.7	0		546	3	0.3	1.3	0.2	97	78 ± 6
	07/05/2009	10.4	5.1	2	14.4	0	45	333	4	0.6	3.8	0.4	120	82 ± 2
	25/07/2009	4.24	6.2	0.5	19.7	0	248	242	4	0.9	1.0	0.4	98	82 ± 3
	30/10/2009	3.67	3.7	1	14.2	8.7	182	384	5	2.3	1.9	0.4	111	82 ± 3
A2	15/02/2009	54.1	4.2	3	7.4	13.7		392	2	0.6	0.2	0.3	79	51 ± 6
	08/05/2009	9.95	5.2	3	14	22.5	39	122	3	0.7	0.2	0.4	44	64 ± 8
	24/07/2009	5.01	6.4	1.5	19.5	27.5	33	47	5	1.1	0.3	1.0	17	42 ± 8
	31/10/2009	3.47	4.5	1	15.5	29.9	33	46	11	1.7	0.3	0.2	29	37 ± 4
A3	16/02/2009	49.7	3.2	1.75	8	20		199	2	0.6	0.1	0.2	53	74 ± 3
	06/05/2009	10.7	4.7	2	13.5	24.6	21	86	3	0.4	0.2	0.3	31	74 ± 3
	26/07/2009	3.59	5.7	3	19.1	30.9	48	25	4	1.0	0.3	0.4	12	71 ± 8
	01/11/2009	4.91	5	2.5	15	33	20	7	4	0.8	0.3	0.1	16	73 ± 1

Table 2: Statistical t-test for seasonal changes of grain size (% < 63 μm) and porosity (ϕ) in surface sediments in the inner Aulne Estuary (station A1, n=3).

	% < 63 μm		ϕ	
	Shapiro test p=0.03		Shapiro test p=0.023	
	t	*p*	*t*	*p*
Feb ~ May	-1.14	0.357	-5.91	0.01
Feb ~ Jul	-1.055	0.367	-6.13	0.021
Feb ~ Oct	-1.176	0.33	-4.72	0.042

Table 3: Correlations between surface sediment properties along the Aulne Estuary (stations A1, A2 and A3). n=12 (P forms) or 36 (dissolved forms). Significant correlations (p<0.5) are in **bold**.

		$(NO_3^-+NO_2^-)$	NH_4^+	PO_4^{3-}	Fe^{2+}	Mn^{2+}	$Si(OH)_4$	ϕ	Fe-P	Aut-P	Det-P
Station A1	NH_4^+	-0.216									
	PO_4^{3-}	0.15	**-0.605**								
	Fe^{2+}	-0.242	**0.741**	**-0.578**							
	Mn^{2+}	**-0.442**	**0.75**	**-0.726**	**0.79**						
	$Si(OH)_4$	**-0.4**	**0.787**	**-0.503**	**0.892**	**0.82**					
	ϕ	0.032	**-0.602**	0.176	**-0.513**	**-0.473**	**-0.644**				
	Fe-P	**0.477**	**-0.525**	0.27	**-0.656**	**-0.558**	**-0.738**	**0.415**			
	Aut-P	-0.088	**0.711**	**-0.736**	**0.695**	**0.575**	**0.674**	**-0.395**	**-0.48**		
	Det-P	-0.273	0.227	**-0.592**	**0.363**	**0.594**	0.266	**-0.362**	**-0.389**	**0.378**	
	Orga-P	**0.479**	**-0.342**	0.251	**-0.396**	**-0.477**	**-0.481**	**0.641**	**0.506**	**-0.335**	**-0.433**
Station A2	NH_4^+	-0.278									
	PO_4^{3-}	-0.193	**0.452**								
	Fe^{2+}	-0.078	-0.025	-0.07							
	Mn^{2+}	-0.207	0.073	-0.095	**0.83**						
	$Si(OH)_4$	-0.24	**0.381**	**0.398**	**0.791**	**0.7**					
	ϕ	0.347	**-0.63**	-0.327	0.091	-0.083	-0.136				
	Fe-P	0.135	**-0.582**	**-0.441**	-0.227	**-0.386**	**-0.471**	**0.369**			
	Aut-P	-0.265	0.014	-0.112	0.056	-0.118	0.109	-0.234	**0.555**		
	Det-P	-0.251	0.049	-0.233	0.093	0.162	0.013	**-0.456**	0.253	**0.336**	
	Orga-P	0.127	-0.179	0.048	0.092	0.112	-0.052	**0.449**	-0.102	**-0.518**	-0.155
Station A3	NH_4^+	-0.237									
	PO_4^{3-}	-0.192	**0.929**								
	Fe^{2+}	-0.247	**-0.497**	**-0.436**							
	Mn^{2+}	**-0.494**	-0.041	-0.045	0.15						
	$Si(OH)_4$	-0.39	**0.934**	**0.835**	-0.259	-0.044					
	ϕ	**0.499**	**-0.408**	-0.273	-0.107	-0.083	**-0.597**				
	Fe-P	**0.305**	**-0.576**	-0.471	0.159	0.236	**-0.678**	**0.646**			
	Aut-P	0.144	0.281	0.204	**-0.349**	-0.109	0.194	0.213	0.098		
	Det-P	-0.269	**0.351**	0.257	-0.266	0.353	**0.291**	0.024	-0.155	**0.307**	
	Orga-P	**0.458**	**-0.367**	**-0.297**	-0.1	**-0.45**	**-0.508**	**0.459**	**0.345**	0.054	**-0.461**

818
819 Table 4: Summary of Aut-P, Fe-P, Orga-P, Det-P concentrations (µmol g^{-1}) and $Si(OH)_4$
820 concentrations (µM) in freshwater, estuarine and marine ecosystems. All P forms were extracted
821 with the SEDEX method (modified or not).

Site	System type	Auth-P	Orga-P	Fe-P	Det-P	$Si(OH)_4$	Reference
			(µmol g^{-1})			(µM)	
Middle Adriatic	marine	0-2.7	1.5-5.4	1.9-11.9	0.4-3.4		Matijević et al. (2009)
Patuxent River Estuary	brackish	1-4.5	4-10	15-55	2-4.5		Jordan et al. (2008)
St Laurent Gulf	marine	8.6-13.6	4-5	7-28		200*	Louchouarn et al. (1997) *Thibodeau et al. (2010)
Amazon River	fresh	4.7	4.5	4.1	2.2		Berner and Rao (1993)
	mixing zone	3.6	4.3	7.5	1.0	50-250*	*Michalopoulos and Aller (2004)
Penzé Estuary	inner estuary	8-12	17	22	up to 8.6		Andrieux-Loyer et al. (2008)
	outer estuary	1.5-2	2	2	4-5		
Yangtze River	fresh	1.7-8.2	0.6-2.8	0.1-3.7	1.1-12.6	200-600*	Rao and Berner (1997) *Aller et al. (1985)

822

Figure legends

Fig. 1: Location of stations A1, A2 and A3 along the Aulne Estuary.

Fig. 2: Aulne River discharge ($m^3\ s^{-1}$) at Chateaulin in 2009. Source: DREAL Bretagne/HYDRO-MEDD/DE. Sampling periods are represented by grey areas.

Fig. 3: Vertical profiles of porosity and tomographic intensity (TI, HU) and bi-dimensional CT scan pictures from the inner to the outer Aulne Estuary (stations A1, A2 and A3, rows) in February, May, July and October 2009 (columns). Horizontal dashed lines illustrate the temporal evolution of specific layers described in the text. Fluid muds and sediment deposition are indicated on CT scan pictures.

Fig. 4: Contour maps of phosphorus forms (rows: Orga-P, Fe-P, Aut-P, Det-P; µmol g^{-1}) in benthic sediments along the Aulne Estuary (columns: A1, A2 and A3) in 2009. Measured values are represented by black points (n=1) in February, May, July and October. The horizontal dashed lines represent the temporal evolution of specific layers observed in Fig. 3.

Fig. 5: Contour maps of dissolved species concentrations (rows: PO_4^{3-}, NH_4^+, $Si(OH)_4$, NO_3^{2-}, Fe^{2+}, Mn^{2+}; µM) in pore waters along the Aulne Estuary (columns: A1, A2 and A3) in 2009. Measured values are represented by black points (n=3) in February, May, July and October.

Fig. 6: Contour maps of dissolved species molar ratios (rows: NH_4^+:PO_4^{3-}, Fe^{2+}:PO_4^{3-}) in pore waters along the Aulne Estuary (columns: A1, A2 and A3) in 2009 (rows). Measured values are represented by black points (n=3) in February, May, July and October.

Fig. 7: Vertical profiles of NH_4^+:PO_4^{3-} and Fe^{2+}:PO_4^{3-} ratios, PO_4^{3-} and $Si(OH)_4$ concentrations

844 (µM), Orga-P, Fe-P and Aut-P concentrations (µmol g^{-1}) at station A1 in February and at station

845 A2 in October.

846

847 *Figures*

848

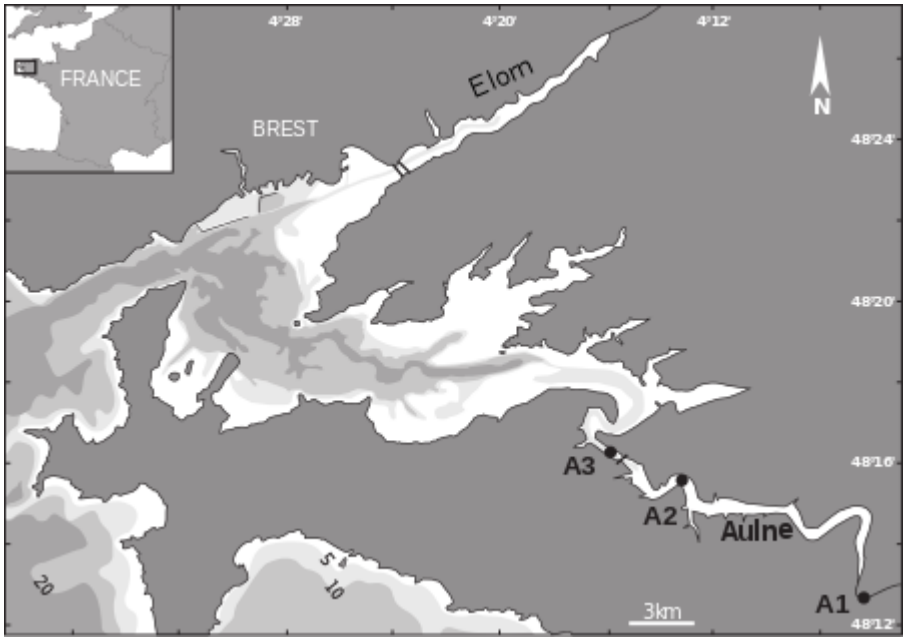

849

850 **Fig. 1**

851

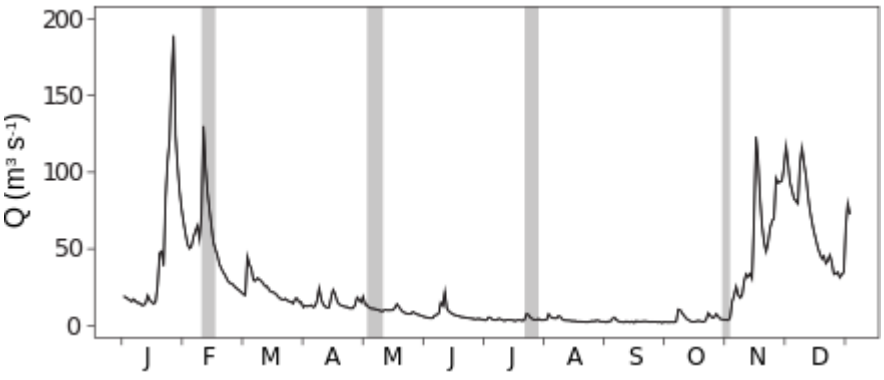

852

853 **Fig. 2**

854

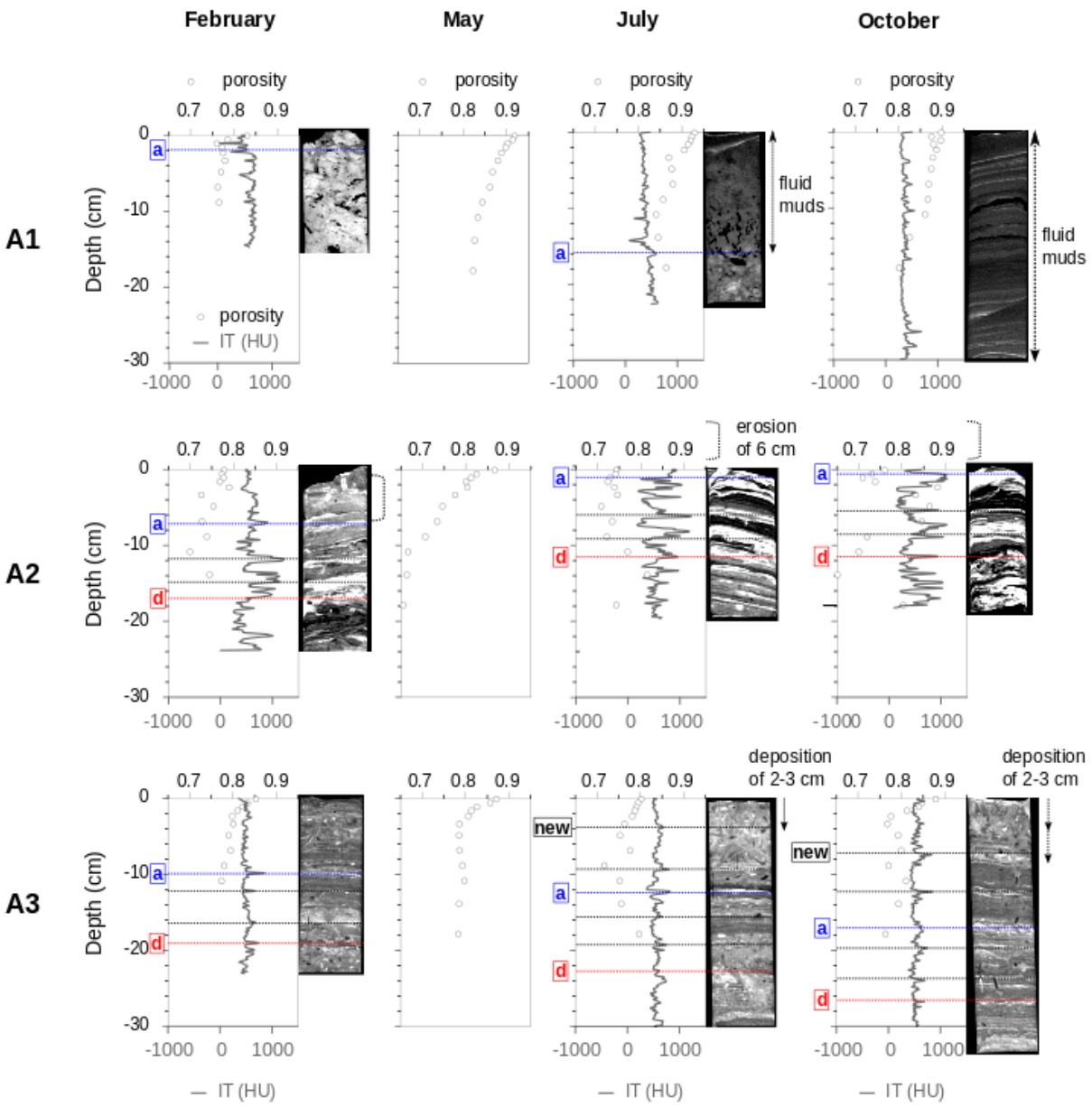

855

856 **Fig. 3**

857

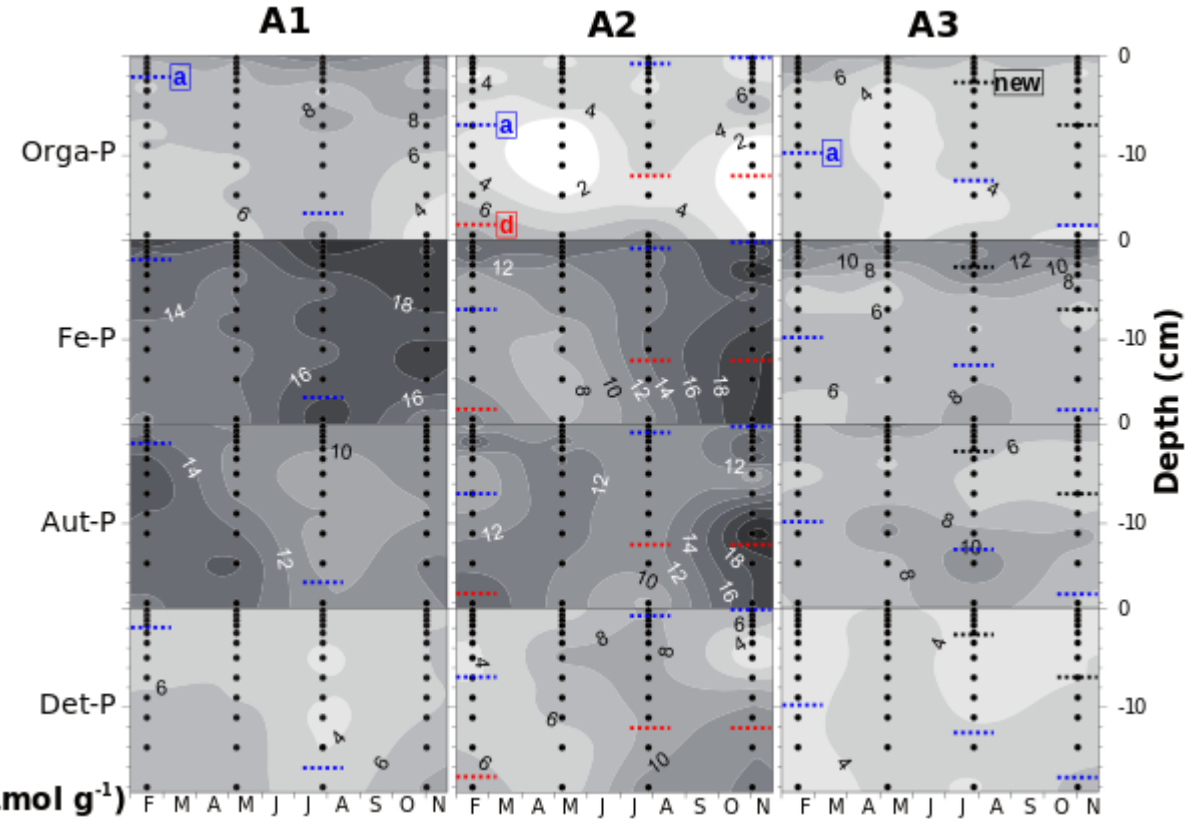

Fig. 4

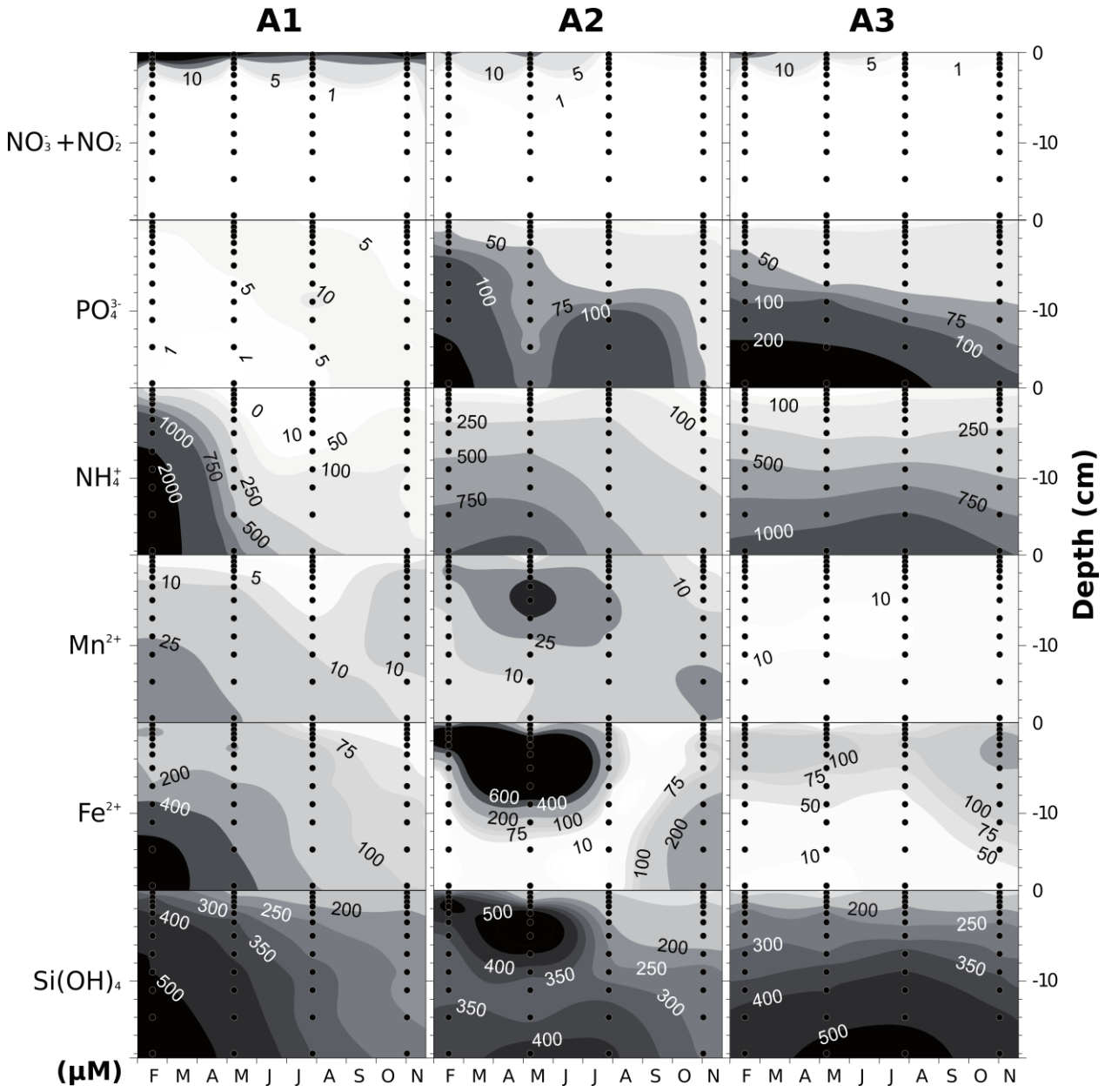

Fig. 5

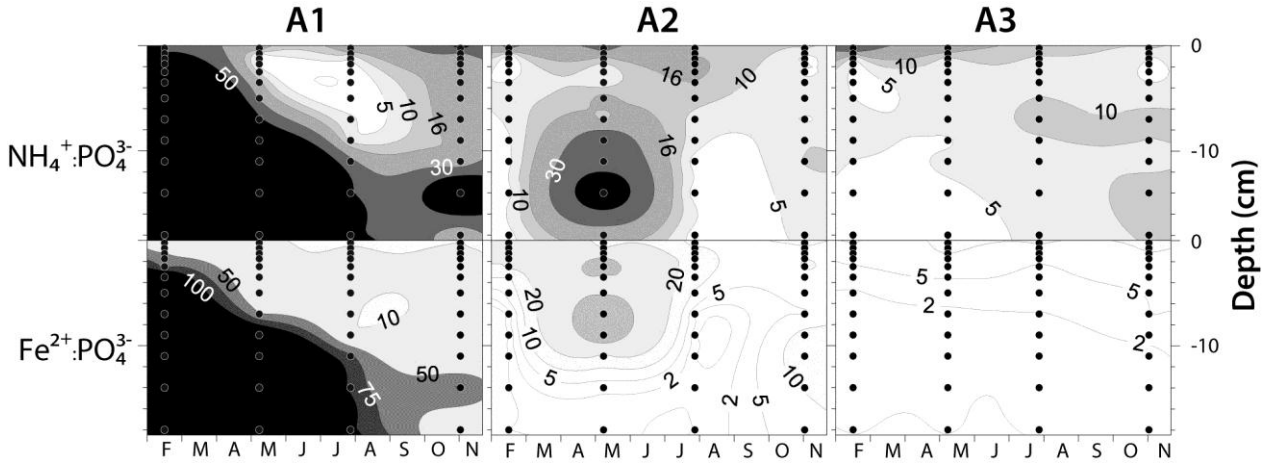
A1
A2
A3
NH_4^+:PO_4^{3-}
Fe^{2+}:PO_4^{3-}
Depth (cm)
0
-10
0
-10
F M A M J J A S O N
F M A M J J A S O N
F M A M J J A S O N

Fig. 6

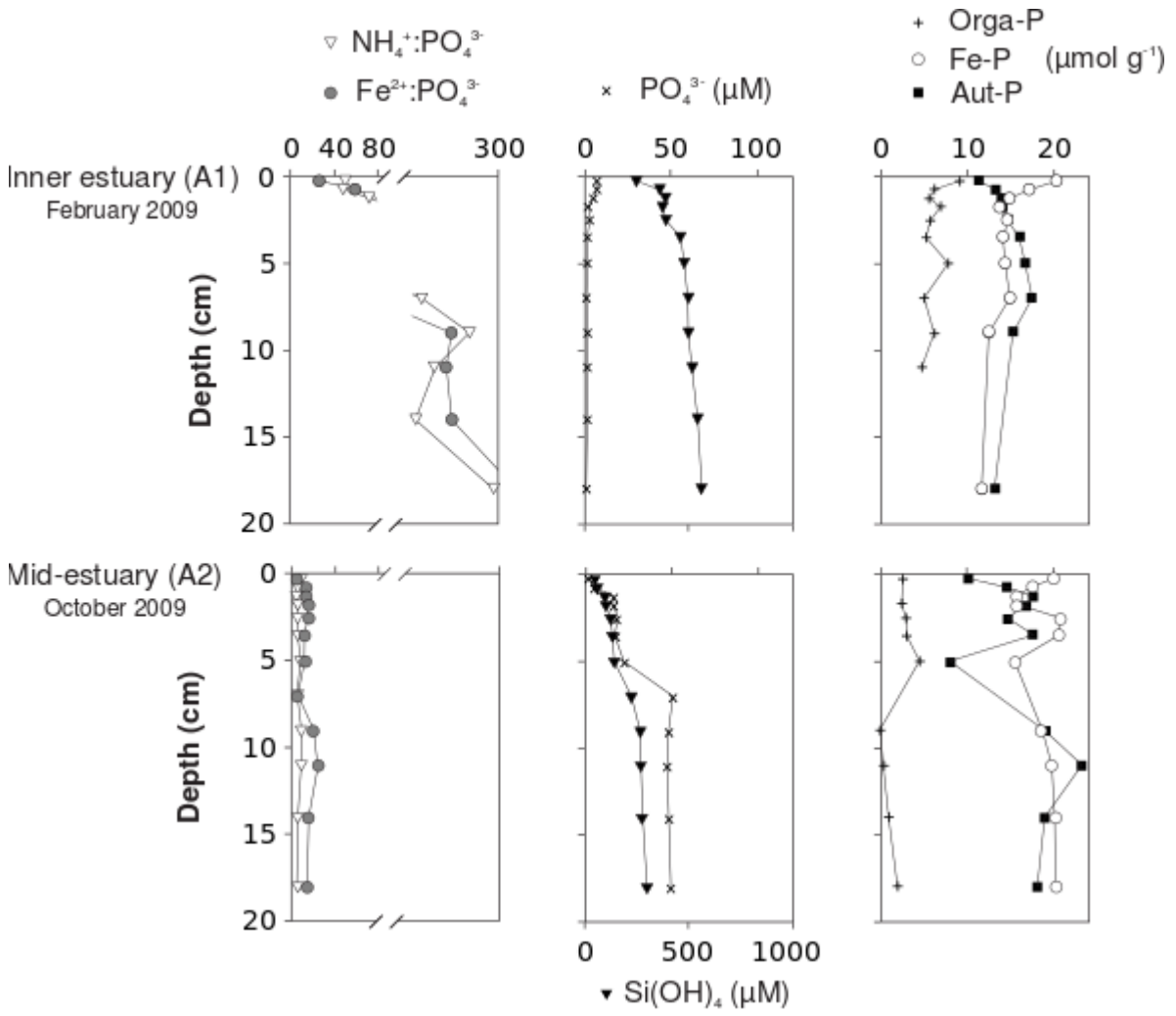
$NH_4^+:PO_4^{3-}$
$Fe^{2+}:PO_4^{3-}$
PO_4^{3-} (µM)
Orga-P
Fe-P (µmol g^{-1})
Aut-P
Inner estuary (A1)
February 2009
Mid-estuary (A2)
October 2009
Depth (cm)
0 40 80 300
0 50 100
0 10 20
0 500 1000
$Si(OH)_4$ (µM)

867

868 **Fig. 7**